Spanish Journal of Agricultural Research
20 (2), e1201, 15 pages (2022)
eISSN: 2171-9292
https://doi.org/10.5424/sjar/2022202-18861
INIA-CSIC

RESEARCH ARTICLE

OPEN ACCESS

Identifying optimal monitoring strategies to predict soil hydraulic characteristics and water contents by inverse modeling

Leonardo E. Scherger[1,2], Javier Valdes-Abellan[3] and Claudio Lexow[2]

[1] *Consejo Nacional de Investigaciones Científicas y Técnicas (CONICET), CCT Bahía Blanca, Argentina.* [2] *Dpt. de Geología, Universidad Nacional del Sur (UNS), Bahía Blanca, Argentina.* [3] *Dpt. de Ingeniería Civil, Universidad de Alicante (UA), Alicante, Spain*

Abstract

Aim of study: To investigate the monitoring strategies that let us to build effective models able to best estimate water contents, θ and pressure heads, h with the least amount of data.

Area of study: Field data was acquired in an experimental plot at Bahía Blanca (Argentina).

Material and methods: Field data of θ(t), h(t) for six soil depth were used to optimize the SHP (θ_r, θ_s, α, n and Ks) by inverse modeling with HYDRUS 1D. Several scenarios of available data from θ(t) and h(t) were considered: (1) six monitoring depths (6-MD); (2) five monitoring depths (5-MD); (3) four monitoring depths (4-MD). Model accuracy was assessed by comparing the measured and predicted θ and h for each monitoring strategy. Additionally, field measured SHP with independent methods were compared to inversely optimized SHP.

Main results: The best fit between predicted and observed θ and h was achieved with the 6-MD strategy. Nevertheless, deterioration of statistics EF and rRMSE in the 5-MD or 4-MD schemes were lower than 10%, depending on the location of the missing data. The observation points that had less importance in parameter prediction corresponded to the intermediate vadose zone and to the deeper layers. The proposed strategies presented a better performance than field measured SHP to reproduce soil water retention curves for each layer of the soil profile.

Research highlights: By reducing the number of vertical observations in the profile without harming the final SHP estimation, the resources needed in data monitoring strategies can be greatly enhanced.

Additional key words: soil monitoring strategy; water management; water flux; vadose zone; HYDRUS.

Abbreviations used: EF (Nash-Sutcliffe coefficient of efficiency); MD (monitoring depth); rRMSE (relative root mean square error); SHP (soil hydraulic properties); SWRC (soil water retention curve); SWS (soil water storage).

Authors' contributions: conception: LES, JVA; acquisition: LES, CL; interpretation of data: LES, JVA, CL; drafting of the manuscript: LES; critical revision of the manuscript: JVA, CL; obtaining funding: CL.

Citation: Scherger, LE; Valdes-Abellan, J; Lexow, C (2022). Identifying optimal monitoring strategies to predict soil hydraulic characteristics and water contents by inverse modeling. Spanish Journal of Agricultural Research, Volume 20, Issue 2, e1201. https://doi.org/10.5424/sjar/2022202-18861

Received: 14 Sep 2021. **Accepted:** 29 Apr 2022.

Funding agencies/institutions	Project / Grant
Universidad Nacional del Sur (UNS)	24/H145
Consejo Nacional de Investigaciones Científicas y Técnicas (CONICET)	---

Competing interests: The authors have declared that no competing interests exist.

Correspondence should be addressed to Leonardo E. Scherger: leonardo.scherger@uns.edu.ar

Introduction

The knowledge of soil hydrological processes is a fundamental tool for a sustainable management of both, soil, and water. Adequate characterization of soil water movement is a very useful tool for many different objectives. Application of numerical models based on physical equations and soil hydraulic properties (SHP) allows predicting hydrological processes that are difficult to measure in the field, such as root water uptake, evaporation, water drainage or groundwater recharge (Filipović *et al.*, 2014; Guo *et al.*, 2018; Yetbarek *et al.*, 2020). These SHP consist of the soil water retention curve (SWRC), which relates soil moisture, θ to soil pressure head, h, and the hydraulic conductivity curve, which relates the conductivity (K) to h or θ (Ramos *et al.*, 2006). Numerous functions have been proposed over the past decades to describe the SHP across the complete range of soil water contents (Khlosi *et al.*, 2008), *e.g.*, those by Brooks & Corey (1964), van Genuchten-Mualem (Mualem 1976; van Genuchten 1980), Durner (1994), Fredlund & Xing (1994), Kosugi (1999) and Groenevelt & Grant (2004). These models

have been reported successful for describing certain parts of the SWRC (*e.g.* wet or dry part), soil textures, regions of the world, or limited soil stress range (Too *et al.*, 2014). Cornelis *et al.*, (2005) compared the performance of the most-widely used analytical expressions for the SWRC in numerous soil textures. In this work, the traditional van Genuchten-Mualem model was chosen, as it has proven its ability to represent the hydrodynamics of a wide variety of soils. Also, the van Genuchten-Mualem model is frequently used as a benchmark for comparison with other works in the literature (Vereecken *et al.*, 2010). Applied simulations depend on the correct election of the SHP. Many different techniques are to date available to determine SHP, however most of them are time consuming and money costly. Direct measurements of SHP mainly consist of field monitoring tasks (Bordoni *et al.*, 2017) and well-known laboratory practices as the pressure plate extractor or the hanging water column method (Dane & Topp, 2002), among others. An alternative to the direct SHP measurement is the use of inverse procedures assisted by soil-water flux models (Schelle *et al.*, 2013; Ventrella *et al.*, 2019; da Silva *et al.*, 2020). These methods require in situ measures such as θ and h in soil profiles. Inverse methods are based on the minimization of an objective function, which expresses the disagreement between observed and predicted values (Šimůnek *et al.*, 1998). This methodology is a simple and quick approach to obtain a calibrated model that represents the real hydraulic dynamics of the soil water.

Several researchers had focused their interest on the variables that can affect the estimations made by inverse modeling. For instance, Abbaspour *et al.* (1999) studied the influence of input-variables, (*e.g.*, water content, pressure heads or water flows) over parameters estimation in lysimeter experiments. Gabriel *et al.* (2019) assessed the medium-term effect of cover crops on soil hydraulic properties. Also, the spatial and temporal variations of field measurements can play an important role in the inverse modeling. Schelle *et al.* (2013) studied local measurement heterogeneities of water contents and pressure heads and their relation to parameter optimization. Similarly, Qu *et al.* (2014) probed that the spatial variation of field measurements correlates with spatial variation in hydraulic parameters. Valdes-Abellan *et al.* (2015) compared two different data acquisition strategies for water potential and water content monitoring at several depths. Furthermore, different modeling strategies and parametrization models of the soil profile have been studied (Thomas *et al.*, 2017; Graham *et al.*, 2018). Nevertheless, there are limited studies on the consequences that scarce data from specific soil depths in the profile has over water fluxes and SHP prediction.

If θ and h are monitored at many different depths, simulations may differ little from real data, as optimization algorithms have a good description of water flow along the complete profile (Musters *et al.*, 2000). However, the resources needed to obtain copious data are sometimes unavailable and questions arise regarding which is the best monitoring strategy that allows for obtaining the best SHP estimation with the fewest number of sensors. On the other hand, when there is null or scarce data for some layers within the soil profile several solutions of the same problem can be encountered. Abbaspour *et al.* (1999) reported that "unique" hydraulic parameters are not valid to be discovered by the right experimental setup, being the behavior of the soil more compatible with the notion of random variables than single-valued soil properties. The estimations made by inverse modeling could vary according to the data available and the vertical distribution of the measurement points in the profile. Even more, available data at a specific soil depth might influence SHP prediction for other depths with no information, and the impact on the layer structure on this influence remains still unclear during the inverse estimation procedure.

The aim of this work was to investigate the impact of reducing observed data (by reducing the number of observation depths) in order to build effective models able to predict observations without a significant reduction in their accuracy. For this purpose, HYDRUS 1D was used to inversely predict SHP (θ_r, θ_s, α, n and Ks) based on field measurements of θ and h from different depths at an experimental plot. Several scenarios of available data were considered to optimize the soil layers SHP for the same temporal series. Comparisons between observed and predicted θ and h were performed to acknowledge the best field monitoring strategies with the fewest number of sensors. If the optimal levels to monitor moisture changes in the soil are recognized, the time, cost, and labor needed for an appropriate soil management practice will be greatly reduced.

Material and methods

Study area

Field measurements were made in Bahía Blanca, Argentina (38°43"S, 62°16"W), in the northwest coast of Bahía Blanca Estuary (Fig. 1). Climatologically, the region is a transition between the sub-humid temperate climate of the Pampas plain and the semi-arid climate of Argentine Patagonia. An average total annual precipitation of 593 mm was determined for the period 1901-2006. Maximum rainfall occurs in spring and autumn and minimum in winter. Scherger *et al.* (2019) estimated the potential evapotranspiration as 1460 mm and the actual evapotranspiration as 398 mm for the period 2011-2015. Natural soils develop from sediments deposited over a wide tidal plain. However, natural conditions are only present as restricted relics since most of the area has been

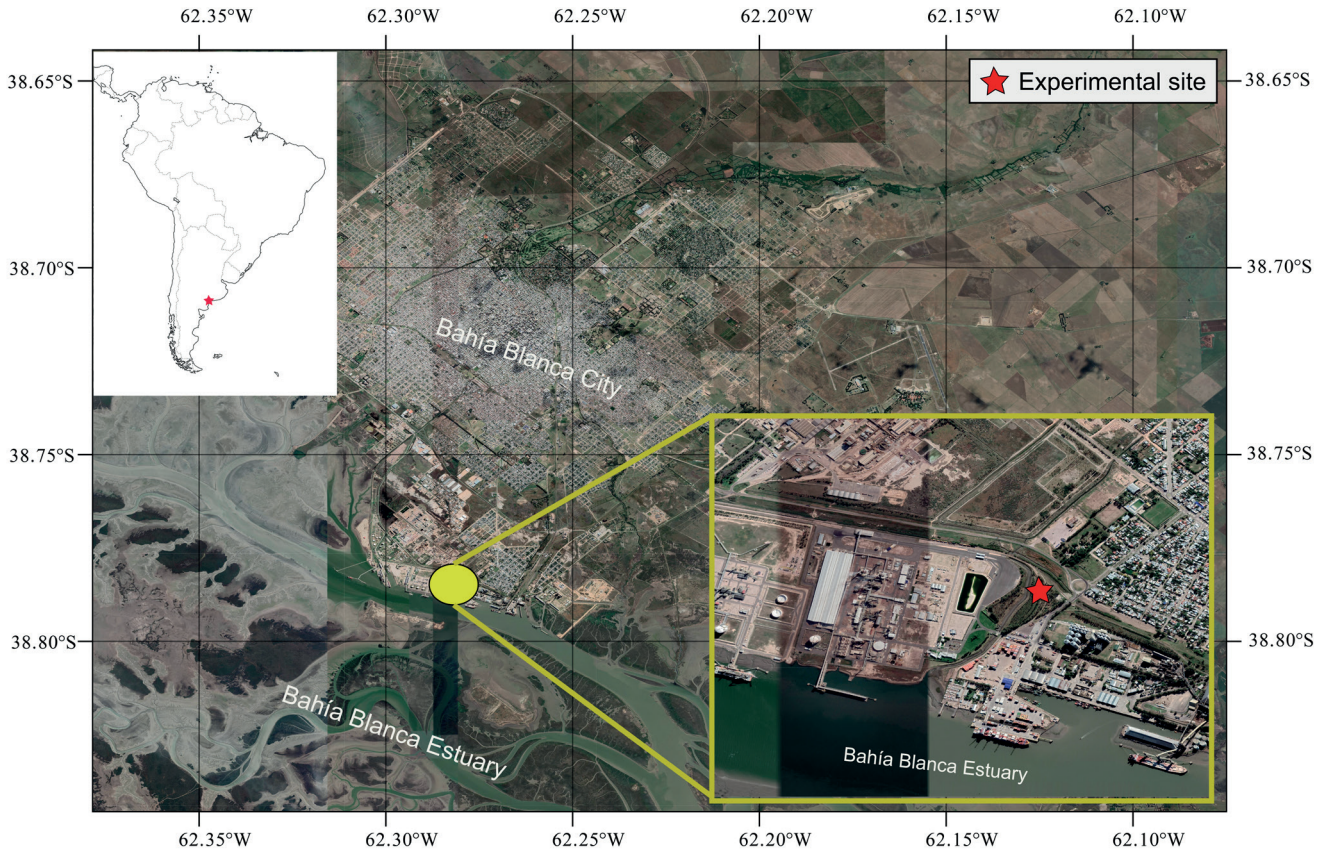

Figure 1. Study area location.

highly modified by human activity. Natural soils were covered with filling material to support industrial buildings and roads network. Filler soils are primary composed by compacted sandy loam and loamy sand sediments.

The plot is located over an unconfined quaternary aquifer of detrital origin. It is composed by silty clay and clayed silt sediments which overlie loess deposits of plio-pleistocene age. Groundwater is classified as hypersaline as salinities values range from 5000 mg L^{-1} to 50000 mg L^{-1}, towards the discharge zone. In natural sectors, the water table has shallow depths, close to one meter. Since the study area was topographically elevated, the unsaturated zone normally has thickness between 2 and 3 meters. Groundwater flow has a N-S direction, releasing the surplus volume into the estuary.

Soil profile characterization

To describe the main characteristics of the soil profile two boreholes were made by means of a helicoidal shovel and disturbed and undisturbed samples were taken from depths of 30, 60, 90, 120, 150 and 180 cm. The main characteristics of the soil profile in the experimental plot are listed in Table 1. Based on field data and physical-chemical properties four layers were defined. Despite, the first three layers were classified as loamy sediments, there were some discrepancies in the measurements of bulk density, saturated hydraulic conductivity, and water retention data to support this decision. Soil bulk density was determined by the core method for each soil layer (Blake & Hartge, 1986). In field, the saturated hidraulic conductivity, Ks was measured by a tension infiltrometer for the soil surface and by the inverse auger hole method for each soil layer (Scherger *et al.*, 2020). The laboratory procedures on sediment samples were as follows. Particle size distribution was evaluated using the pipet method (Gee & Bauder, 1986). Total organic carbon (TOC) was measured by dry combustion using a LECO CR-12 Carbon System Analyzer model 781-600. Carbonate content was determined according to Bernard's method by means of a direct calcimeter reading (Hulsemann, 1966).

The plot presented a sparsely distributed grazing-pasture type soil cover. The percentage of soil covered by plants was estimated as 70% according to field observations in the experimental plot.

The field measured SHP to be optimized by inverse modeling are presented in Table 1. The initial value for θ_r, θ_s, α and n from the van Genuchten model, were estimated from Rosetta (Schaap *et al.*, 2001). This pedotransfer function was obtained from a large number of soil hydraulic data and soil properties from three soil databases derived from soils in template to subtropical climates of North America and Europe. The initial

Table 1. Soil profile characteristics and field measured soil hydraulic properties (SHP) used as initial estimates in the numerical model.

	Depth (cm)			
	0–40	**40–70**	**70–110**	**110–200**
Sand (%) [1]	56.9	72.7	53.6	87.8
Silt (%) [1]	37	24.5	42.7	10.5
Clay (%) [1]	6.1	1.9	3.7	1.7
Soil texture	sandy loam	loamy sand	sandy loam	sand
pH [2]	9.6	9.2	9.1	9.1
ρ_b (g cm^{-3})	1.41	1.44	1.5	1.48
Φ (-) [3]	0.46	0.45	0.43	0.44
K_s (cm d^{-1}) [4]	132.8	56.8	7.6	40.1
K_s (cm d^{-1}) [5]	128.4	-	-	-
TOC (%) [6]	0.22	0.05	0.02	0.06
$CaCO_3$ (%) [7]	4.8	5.2	1.8	0.26
	Field measured SHP			
θ_r (-) [8]	0.010	0.010	0.118	0.010
θ_s (-)[9]	0.455	0.360	0.356	0.413
α (cm^{-1}) [10]	0.0096	0.0067	0.0196	0.0212
n (-) [11]	1.993	2.028	1.638	3.656

[1] Grain size distribution: sand (2.00–0.05 mm), silt (0.05–0.002 mm) and clay (<0.002 mm). [2] Measured in a 1:2.5 soil/water solution ratio. [3] Φ: Total soil porosity. [4] K_s: saturated hidraulic conductivity measured by inverse auger hole method. [5] K_s: saturated hidraulic conductivity measured by tension infiltrometer. [6] TOC: total organic content. [7] $CaCO_3$: calcium carbonate content. [8] θ_r: residual water content. [9] θ_s: saturated water content. [10] α: inverse of the air-entry suction. [11] n: porosity distribution index.

values for θ_r, θ_s, α and n were predicted according to soil texture and bulk density. Rosetta also allows the inclusion of water retention points to estimate van Genuchten parameters (Scherger *et al.*, 2020). The soil water retention curve-fit code RECT (van Genuchten *et al.*, 1991) was used to optimize the Rosetta estimation including field retention data, θ(h). Otherwise, the initial saturated hydraulic conductivity (Ks) for each layer corresponded to the value measured in field by the inverse auger hole method (Table 1). Field measured SHP with independent methods were later compared to inversely optimized values to assess model validity.

Experimental design

Field data were acquired from 04/August 2017 to 20/February 2020. The equipment present in the plot consists of two tensiometer sets (SoilSystemCorp.), installed at depths of 30, 60, 90, 120, 150 and 180 cm, and a continuous recording phreatimeter (LF-10) installed at a monitoring well. Soil moisture was simultaneously monitored by gravimetric sampling for the same soil depths. Accordingly, the volumetric soil water content, θ was calculated based on the bulk density of each layer. Field data was monitored on a monthly time scale. A schematic design of the plot is shown in Fig. 2.

The variables θ and h were monitored for six soil depths. Field data was later used to optimize the SHP by inverse modeling.

Meteorological data of precipitation, relative humidity, wind speed, temperature and solar radiation were acquired in a meteorological station located one kilometer apart from the experimental site.

Inverse model

Theoretical models

The soil water retention and hydraulic conductivity curves were model according to van Genuchten-Mualem (Mualem, 1976; van Genuchten, 1980) constitutive equations:

$$S_e = \frac{\theta(h)-\theta_r}{\theta_s-\theta_r} = [1+(\alpha h)^n]^{-m} \quad [1]$$

$$K(h) = K_s S_e{}^l \left[1-(1-S_e{}^{\frac{1}{m}})^m\right]^2 \quad [2]$$

where S_e is the effective saturation, θ_r and θ_s [L^3 L^{-3}] are residual and saturated water contents, α [L^{-1}] is related to

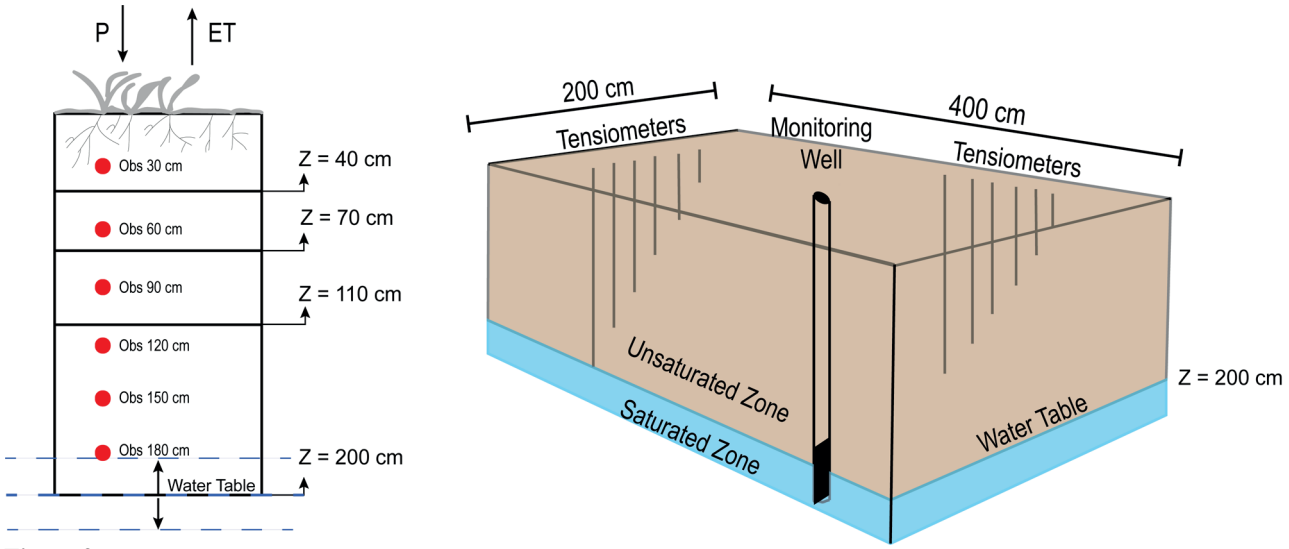

Figure 2. Schematic design of the experimental plot and soil profile.

the inverse of the air-entry suction (ha), n and m [-] are empirical parameters dependent on soil properties, where m=1–1/n, and l [-] is the pore conductivity, which has a value of 0.5 as an average of different soils (Mualem, 1976).

The reference evapotranspiration (ET_0) was calculated by the Penman-Monteith method (Allen *et al.*, 1998). To discriminate the ET_0 into transpiration and bare soil evaporation the dual crop coefficient approach was applied:

$$ET_c = (K_{cb} + K_e)ET_0 = T_p + E_p \qquad [3]$$

where K_{cb} is the crop basal coefficient [-], K_e is the evaporation coefficient [-], T_p is the potential transpiration [L T^{-1}] and E_p is the potential evaporation [L T^{-1}]. The K_{cb} value was chosen as 0.7 and corresponded to a grazing pasture crop in mid-season/end-season stage of growth.

The root water uptake model was described by Feddes *et al.* (1974):

$$S = \alpha(h)S_p \qquad [4]$$

where $\alpha(h)$ is a dimensionless water stress response function ($0 \leq \alpha \leq 1$) and S_p is the potential water uptake. Root water uptake is null under or near soil saturation (h_1) or under pressure heads greater than the wilting point (h_4). Transpiration rate is maximum as α equals 1 when $h_2<h<h_3$. For the ranges of $h_4<h<h_3$ and $h_2<h<h_1$, transpiration decrease linearly as the pressure head decrease or increase, respectively. The values for the current crop were taken from Wesseling (1991) for pastures (h_1= -10 cm; h_2= 25 cm; $h_{3.1}$= -200 cm; $h_{3.2}$= -800 cm; and h_4 = -8000 cm). A maximum rooting depth of 30 cm was considered for this perennial crop.

Numerical model

Soil water contents and pressure heads were simulated with HYDRUS 1D software (Šimůnek *et al.*, 2013). The HYDRUS program numerically solves the Richards equation for variably- saturated water flow.

$$\frac{\partial\theta}{\partial t} = \frac{\partial}{\partial z}\left(K\left(\frac{\partial h}{\partial z} + 1\right)\right) - S \qquad [5]$$

where θ is the volumetric water content [L^3 L^{-3}], t is time [T], z is the vertical dimension [L], K is the unsaturated hydraulic conductivity [L T^{-1}], h is the pressure head [L], and S is a sink term that represents water uptake by plants [L^3 L^{-3} T^{-1}].

The depth of the simulation profile was 200 cm, which was discretized into a grid size of 2 cm (101 nodes). The increase in the number of nodes did not significantly affect model output hence this number of nodes were considered adequate. Simulations were made on a daily time scale during the period from August 2017 to February 2020 (931 days). The time discretization was as follows: initial time step 0.001 days, minimum time step 10^{-5} days and maximum time step 5 days. The initial conditions corresponded to water content measurements in the soil profile for the starting time of the simulations (4 August 2017). Dataset was divided into a parameterization and a validation dataset. The first one included θ(t) and h(t) measurements from day 1 to 697 and the second one from day 698 to 931.

An atmospheric boundary condition was considered for the upper boundary and a variable pressure head boundary condition for the lower boundary. The variable boundary conditions input data required by the model were precipitation, potential evapotranspiration, and groundwater level.

The vertical domain was divided into four layers, according to textural and physical-chemical properties of the soil profile. The final SHP were inversely optimized based on θ(t) and h(t) temporal data sets from each observation points in the soil profile. SHP optimization by inverse solution is based on the minimization of error between observed and predicted values. User-entered initial estimates are iteratively optimized until the highest possible precision is achieved. Solution is accomplished by the Levenberg-Marquardt method, which it is based on least-squares solution approach (Marquardt, 1963). The objective function (Φ) to be minimized during the parameter estimation process may be defined as (Šimůnek *et al.*, 2013):

$$\Phi(\theta,\beta) = \sum_{j=1}^{m} v_j \sum_{i=1}^{kj} w_{i,j}\left[(q_{obs,i}(z_i,t_i) - q_{pred,i}(z_i,t_i,\beta)\right]^2 [6]$$

where $qo_{bs,i}(z_i,t_i)$ represents specific measurements at time ti for the jth measurement set at location z_i and $q_{pred,i}(z_i,t_i,\beta)$ are the corresponding model predictions for the vector of optimized parameters β (*e.g.*, θ_r , θ_s, α, n, and K_s), v_j and $w_{i,j}$ are weights associated with a particular measurement set or point, m is the number of different sets of measurements, and k is the number of measurements in a particular measurement set.

HYDRUS allows users to optimize up to 15 parameters simultaneously. However, when too many parameters are optimized at the same time, the problem often becomes nonunique (Šimůnek & Hopmans, 2002). To minimize issues of uniqueness in the inverse solution, we decreased the number of simultaneously optimized parameters, and a sequential inverse procedure was performed in seven steps (Yakirevich *et al.*, 2010; Valdes-Abellan *et al.*, 2015). Initially, the parameters search (θ_r, θ_s, α, n, and K_s) was done only for the first layer and the remaining parameters were fixed as the initial estimates by using experimentally measured values. The next step was to optimize the parameters for the second layer. Then, the parameters for layers 1 and 2 were searched, simultaneously. At the 4th step, the parameters were adjusted only for layer 3. The procedure continued by increasing the number of layers involved, until all parameters were optimized at the 7th step.

Modeling strategy

Comparisons of different monitoring strategies were made to assess the effect that missing information had on the prediction of SHP by inverse modeling. First, parameter optimization was carried out with all field data acquired at six monitoring depths (6-MD) (30 cm, 60 cm, 90 cm, 120 cm, 150 cm, and 180 cm). This case represented the scenario with the highest number of observations, as 240 registers from θ(t) and h(t) were available as entry data for inverse solution. The next step was to consider that only five monitoring depths (5-MD) were available (n=200). Thus, six simulations were performed subtracting the information from one node at a time. Finally, only four monitoring depths (4-MD) were considered (n=160), subtracting the information from two soil depths, simultaneously. For this scenario, fifteen inverse processes were carried out given all possible combination when removing two depths out of six.

Goodness-of-fit assessment

The performance of the model output for each simulated scenario was assessed by the comparison of the measured and predicted values of water contents, pressure heads and soil water storage. The soil water storage (SWS) was calculated as:

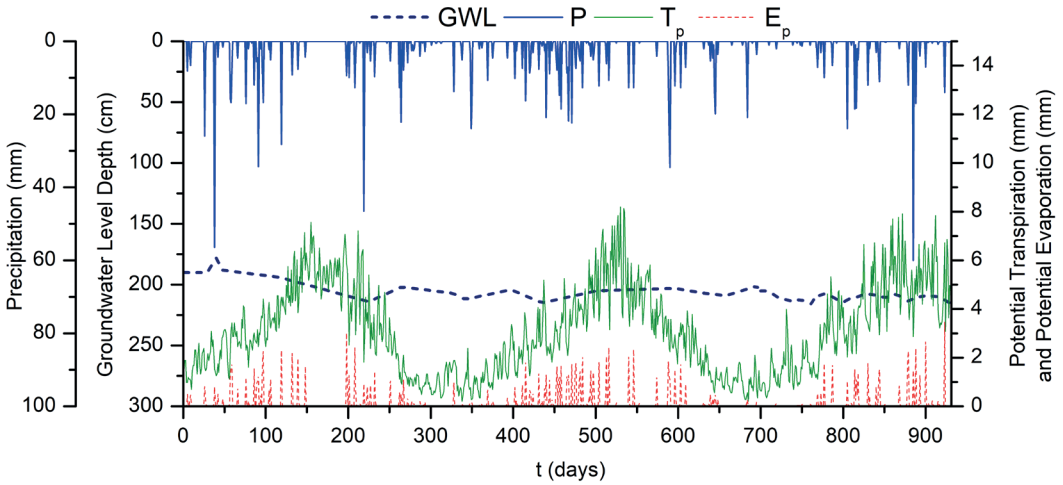

Figure 3. Daily precipitation (P), potential transpiration (T_p), potential evaporation (E_p) and groundwater level (GWL) depth determined during the monitored period.

$$SWS = \sum_{i=1}^{N} \theta_i * z_i \quad [7]$$

where θ_i is the volumetric water content ($cm^3\ cm^{-3}$), z_i is the soil thickness (cm) for the i^{th} soil interval and N is the number of soil intervals. The SWS was calculated for six soil intervals, each one corresponding to field observation points in the profile. The goodness of fit was evaluated by the statistical indicators: Nash-Sutcliffe coefficient of efficiency (EF) (Nash & Sutcliffe, 1970) and relative root mean square error (rRMSE).

$$EF = 1 - \frac{\sum_{i=1}^{N}(X_i^{obs} - X_i^{pred})^2}{\sum_{i=1}^{N}(X_i^{obs} - X_{mean})^2} \quad [8]$$

$$rRMSE = \frac{\sqrt{\frac{1}{N}\sum_{i=1}^{N}(X_i^{obs} - X_i^{pred})^2}}{(X_{max} - X_{min})} \quad [9]$$

where X_i^{obs} and X_i^{pred} are the observed and predicted values, respectively, N is the number of observed values, X_{max} and X_{min} are the maximum and minimum observed values respectively.

The coefficient of efficiency (EF) has been widely used to evaluate the performance of hydrological models. The index ranges from minus infinity to 1.0, with higher values indicating better agreement (Legates & McCabe, 1999). If EF > 0.5 the performance of the model is considered satisfactory (Thomas *et al.*, 2017). On contrary, the optimal value for rRMSE is zero, indicative of a perfect fit between observed and predicted values. When rRMSE values are < 0.1, between 0.1 – 0.2, between 0.2 – 0.3, and > 0.3, the simulation performance is excellent, good, fair, and poor, respectively (Wang *et al.*, 2021). Goodness-of-fit was evaluated using all observed data, including the data employed for the inverse modelling process. The observed and predicted values for soil moisture, SWS and pressure head were compared for the six-monitoring depths (30 cm, 60 cm, 90 cm, 120 cm, 150 cm, and 180 cm) for 18 dates (n=108).

The agreement between field measured SHP and inversely optimized SHP for each modeling strategy was quantified by the rRMSE. The statistical index was calculated by comparing the measured and predicted θ by the soil hydraulic curves (SWRCs) at specific *h*.

Results

Field measurements

Figure 3 shows the daily atmospheric fluxes (precipitation, potential transpiration, and potential evaporation) and groundwater level depths during the monitored period. Rainfalls mostly occurred during spring and autumn, and summer and winter were the dry periods. Potential evapotranspiration was maximum during the summer and minimum in winter. The mean unsaturated thickness was 205 cm, as the groundwater level fluctuated between the depths of 178 cm and 215 cm.

The monitored θ and *h* during the period are included in Fig. 4. Measured θ varied according to the monitored depth in the profile. The greatest water content variations were registered in the upper layers (0-70 cm), as the minimum and maximum values were 0.08 $cm^3\ cm^{-3}$ and 0.32 $cm^3\ cm^{-3}$, respectively. The upper layers were influenced by the atmospheric conditions, and consequently cyclical wetting and drying events were observed. At greater depths, water content variation was reduced. The mean θ measured at 90 cm and 120 cm were 0.25 $cm^3\ cm^{-3}$ (±0.06 $cm^3\ cm^{-3}$) and 0.10 $cm^3\ cm^{-3}$ (±0.03 $cm^3\ cm^{-3}$), respectively. In the deepest layer, water contents were probably influenced by the presence of the water table. The progressive increase in water contents from 120 cm to 180 cm can be related to the proximity to the capillary fringe and the saturated zone.

Pressure heads ranged between 0 cm and -600 cm. Maximum absolute *h* values were monitored in the upper layers and minimum in the lower layer. The sandy layer registered pressure heads in the range of 0 to -100 cm. As the monitored depth increased *h* decreased related to the position of the water table, as explained before for θ.

Numerical simulations with HYDRUS

Six-monitoring depth scenario

Figure 4 shows the simulated θ and *h* for the 6-MD strategy. The model correctly represents the hydrodynamic behavior of the soil profile. The statistical indexes for the calibration and validation steps of the inverse numerical process are listed in Table 2. During the parametrization step, EF presented values higher than 0.75 and the rRMSE had values lower than 0.15 for θ, *h* and SWS. Overall, model validation showed good agreement with field data, especially for the simulated water contents. The mean simulated SWS only differed by -0.7% from the measured value. Simulated pressure heads for the observation points of 30 cm and 60 cm diverge from the measured values, an effect that could be linked to the low temporal frequency of field measurements. Given that the hydrological variables were monitored on a monthly scale, future studies could incorporate continuous recording sensors, for both θ and *h*, which would improve the performance of model simulations.

The inversely optimized SHP for the 6-MD strategy are listed in Table 3. θ_r optimized values were always higher than the initial estimate, parameter range between

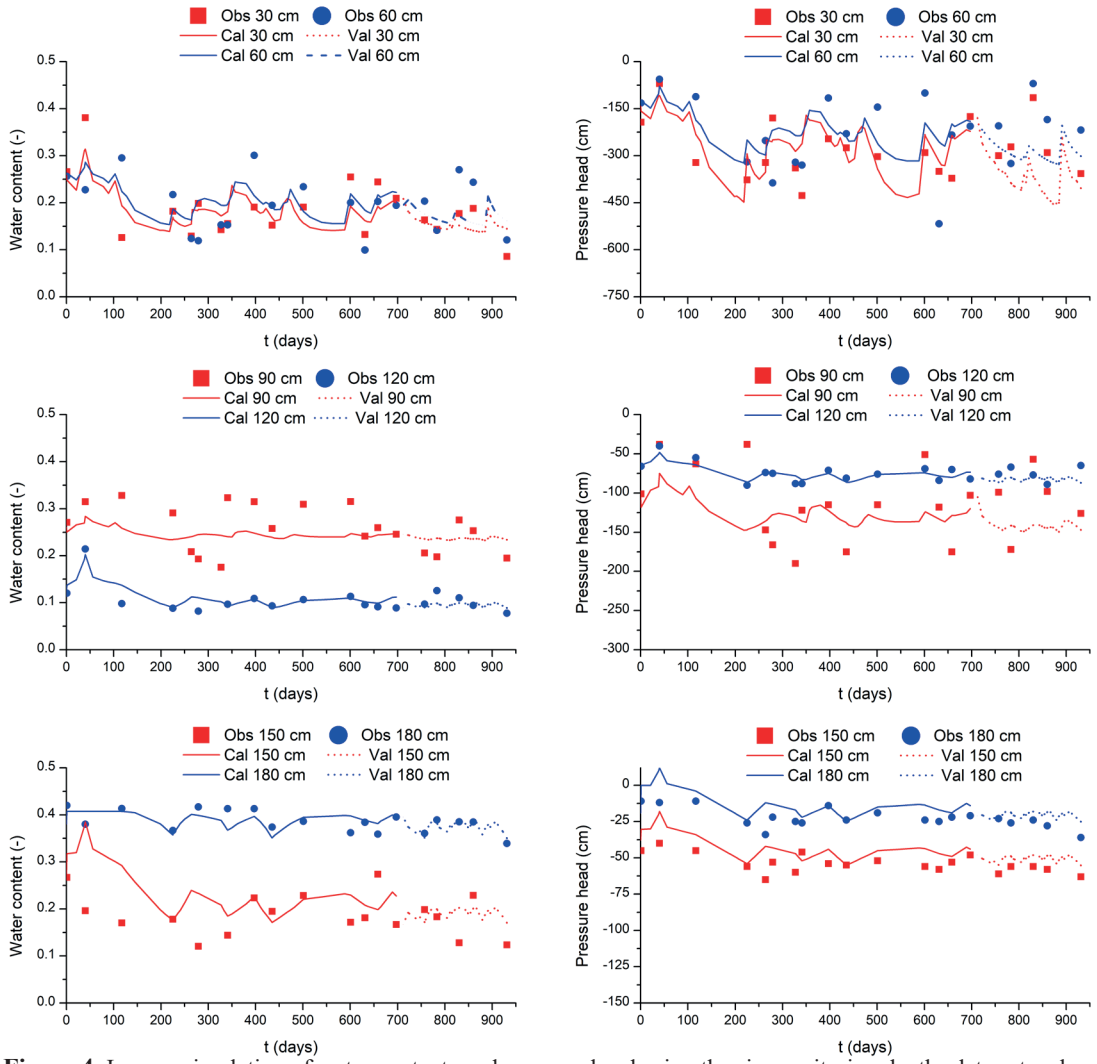

Figure 4. Inverse simulation of water contents and pressure head using the six monitoring depths data sets: observed (Obs) and predicted values for calibration (Cal) and validation steps (Val).

0.02 and 0.12 cm^3 cm^{-3} for the four layers. θ_s was equal to the estimated total porosity (Φ = 0.46) in layer 1, and lower than the measured total porosity in the rest of the layers. The parameter α showed slight variations from the initial estimate, as the optimized value differs only less than 0.005 for all layers. Similarly, the parameter n presented values in the typical range for these types of materials (1.46 and 2.38 for layers 1 and 3 (sandy loam), 2.40 for layer 2 (loamy sand) and 3.20 for layer 4 (sand)) according to Rosseta. The predicted values for Ks were lower than the measured values for all layers, except for layer 4.

Five-monitoring and four-monitoring depths scenarios

The simulations for 5-MD or 4-MD strategies had in all cases lower performances than the 6-MD strategy. The goodness of fit of the inverse model in each scenario for both, θ and h are listed in Table 4; those values were cal-

Table 2. Goodness of fit (coefficient of efficiency, EF and relative root mean square error, rRMSE) for observed and simulated water contents (θ), pressure heads (h) and soil water storage (SWS) for the 6-monitoring depths strategy.

	6-Monitoring depths							
	θ		h		θ and h		SWS	
	EF	rRMSE	EF	rRMSE	EF	rRMSE	EF	rRMSE
Calibration	0.763	0.142	0.754	0.113	0.759	0.128	0.867	0.122
Validation	0.831	0.122	0.339	0.238	0.585	0.180	0.874	0.107

Table 3. Inversely optimized soil hydraulic parameters (SHP) for the six-monitoring depth (6-MD) scenario.

Inversely optimized SHP					
Soil layer	**θ_r (-)[1]**	**θ_s (-)[2]**	**α (cm^{-1})[3]**	**n (-)[4]**	**Ks ($cm\ d^{-1}$)[5]**
1	0.098	0.460	0.0109	2.3774	32.5
2	0.028	0.300	0.0048	2.4052	20.0
3	0.023	0.362	0.0159	1.4654	3.4
4	0.027	0.407	0.0262	3.1999	136.8

[1] θ_r: residual water content. [2] θ_s: saturated water content.[3] α: inverse of the air-entry suction. [4] n: porosity distribution index. [5] Ks: saturated hydraulic conductivity.

culated considering all observation depths and not only the data used for inverse modelling. Two classes were highlighted to identify the observation points whose removal generated less variation in the model performance. One included the cases where the decrement of statistics EF and rRMSE was lower than 5%, and the other those in which model performance deterioration was between 5% and 10%. In all cases, comparisons were made in relation to the 6-MD strategy fit (Table 2) during the parametrization step of the inverse procedure.

For the 5-MD strategies the best performance was achieved by removing the information from depths of 90 cm, 120 cm, or 150 cm. In these cases, the EF was between 0.715-0.717 and the rRMSE ranged from 0.132-0.133, which could be classified as a good fitting, even thought they were worse than the fitting for the 6-MD strategy. Statistics reported a worse fit when removing data from the uppermost and lowermost layers. This effect is directly related to the natural hydrodynamics of the soil profile. As observed in the monitored data, θ and h were influenced by both the atmospheric conditions in the upper part of the domain, and the presence of a shallow water table in the lower domain. Observed data from the two upper monitoring depths (30 and 60 cm) were important to define θ and h variation related to the water entry as precipitation or water exit as evapotranspiration through the upper boundary. Otherwise, the bottom monitoring depth was important to capture the capillarity fringe and processes like recharge or capillary rise.

For the 4-MD strategy, the best performance was accomplished by suppressing data from 30 & 120 cm, 90 & 120 cm, or 90 & 150 cm. In these scenarios, the statistical indexes variation was lower than 5%. When the observation points of 60 & 120 cm were simultaneously removed, the deterioration of the model was between 5% and 10%. In the rest of the scenarios, the model performance was poor and should not be considered as valid field monitoring strategies.

A similar analysis was done for the soil water storage variable to accurately evaluate the optimal monitoring depths in the soil profile. A satisfactory performance of the inverse modeling should be determined for the SWS

Table 4. Goodness of fit (coefficient of efficiency, EF and relative root mean square error, rRMSE) for observed and simulated θ and h for the five-monitoring (5-MD) and four-monitoring (4-MD) depths strategies. Differences with the statistics for the 6-MD lower than 5% are 10% are marked as * and ** respectively.

	θ and h					
	5-Monitoring depths (5-MD)					
	30 cm	**60 cm**	**90 cm**	**120 cm**	**150 cm**	**180 cm**
EF	0.691**	0.676	0.715*	0.715*	0.717*	0.687**
rRMSE	0.140**	0.138**	0.132*	0.132*	0.133*	0.141
	4-Monitoring depths (4-MD)					
	30&60 cm	**30&90 cm**	**30&120 cm**	**30&150 cm**	**30&180 cm**	**60&90 cm**
EF	0.601	0.611	0.716*	0.544	0.583	0.639
rRMSE	0.159	0.159	0.133*	0.167	0.164	0.148
	60&120 cm	**60&150 cm**	**60&180 cm**	**90&120 cm**	**90&150 cm**	**90&180 cm**
EF	0.683**	0.633	0.645	0.705**	0.707**	0.607
rRMSE	0.142	0.149	0.149	0.136**	0.135**	0.158
	120&150 cm	**120&180 cm**	**150&180 cm**			
EF	0.561	0.635	0.650			
rRMSE	0.168	0.153	0.151			

and both, θ and h. Table 5 summarizes the goodness of fit of the simulated soil water storages for all the 5-MD and 4-MD scenarios. In the case of 5-MD, the best model performance was achieved by removing the information from 60 cm, 90 cm, 120 cm, or 150 cm. However, when the data set of 60 cm was not considered, the general performance of the model (both, θ and h) was poorer than cases when suppressed data corresponded to 90 cm, 120 cm, or 150 cm. Thus, the observation point of 60 cm is necessary to predict h in the upper layers of the soil profile. In the scenarios of 4-MD, the only combinations of suppressed data that had a satisfactory performance were the cases when data removal was from monitoring depth of 90 & 120 cm, or 60 & 150 cm. In these two scenarios, statistical indexes variation was lower than 5% in comparison with the 6-MD strategy. However, as explained above when the observation point of 60 cm was suppressed the general model performance decreased, so this case is also discarded as a potential field monitoring strategy. Figure 5 shows the observed and predicted soil water storages for eighteen dates from the temporal series. For the 4-MD scenarios, only the cases that had a satisfactory performance (differences in the statistics < 5% in relation to 6-MD) were illustrated. In the 5-MD cases, as shown previously the worst adjustment corresponds to the suppression of the upper and lower observation points. In the first case, the mean predicted SWS was 444 mm (3.5% lower than observed value) and for the second one, the mean

Table 5. Goodness of fit (coefficient of efficiency, EF and relative root mean square error, rRMSE) for observed and simulated soil water storages (SWS) for the five-monitoring (5-MD) and four-monitoring (4-MD) depths strategies. Differences with the statistics for the 6-MD lower than 5% are 10% are marked as * and ** respectively.

	SWS					
	5-Monitoring depths (5-MD)					
	30 cm	**60 cm**	**90 cm**	**120 cm**	**150 cm**	**180 cm**
EF	0.771	0.866*	0.843*	0.845*	0.833*	0.780
rRMSE	0.140	0.107*	0.116*	0.115*	0.119*	0.137
	4-Monitoring depths (4-MD)					
	30&60 cm	**30&90 cm**	**30&120 cm**	**30&150 cm**	**30&180 cm**	**60&90 cm**
EF	0.688	0.608	0.803**	0.716	0.645	0.816**
rRMSE	0.163	0.183	0.130**	0.156	0.174	0.125*
	60&120 cm	**60&150 cm**	**60&180 cm**	**90&120 cm**	**90&150 cm**	**90&180 cm**
EF	0.809**	0.824*	0.785**	0.826*	0.813**	0.638
rRMSE	0.128*	0.123*	0.136	0.122*	0.141	0.176
	120&150 cm	**120&180 cm**	**150&180 cm**			
EF	0.677	0.702	0.711			
rRMSE	0.166	0.160	0.157			

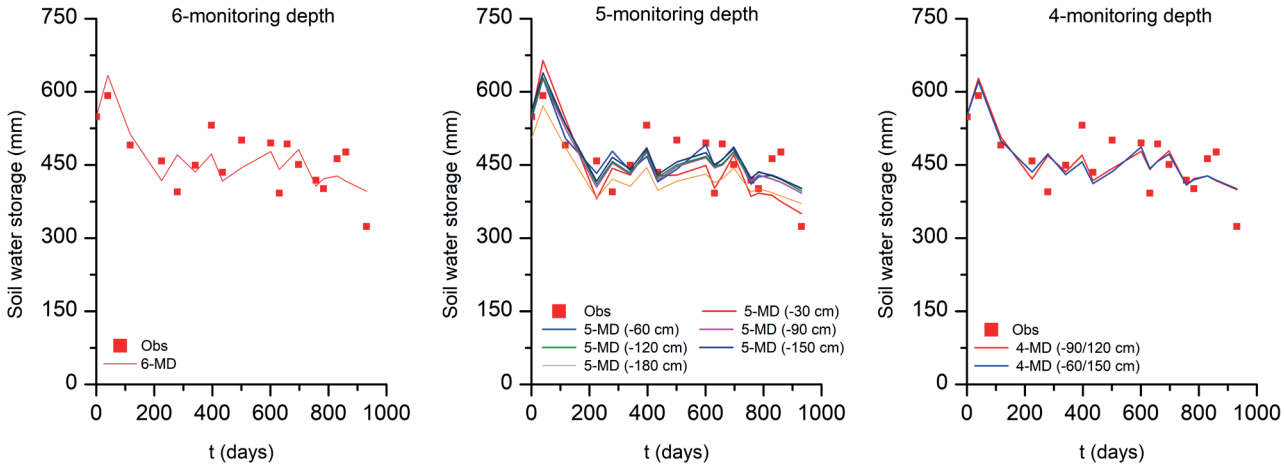

Figure 5. Observed (Obs) and predicted soil water storage for the soil profile (0-200 cm) for each inverse modeling monitoring scheme: with all 6 sampling depths (6-MD), all the scenario with five sampling depths (5-MD) and the best fit scenarios with four (4-MD) sampling depths. The numbers in parentheses indicate the sampling depth excluded in each scheme.

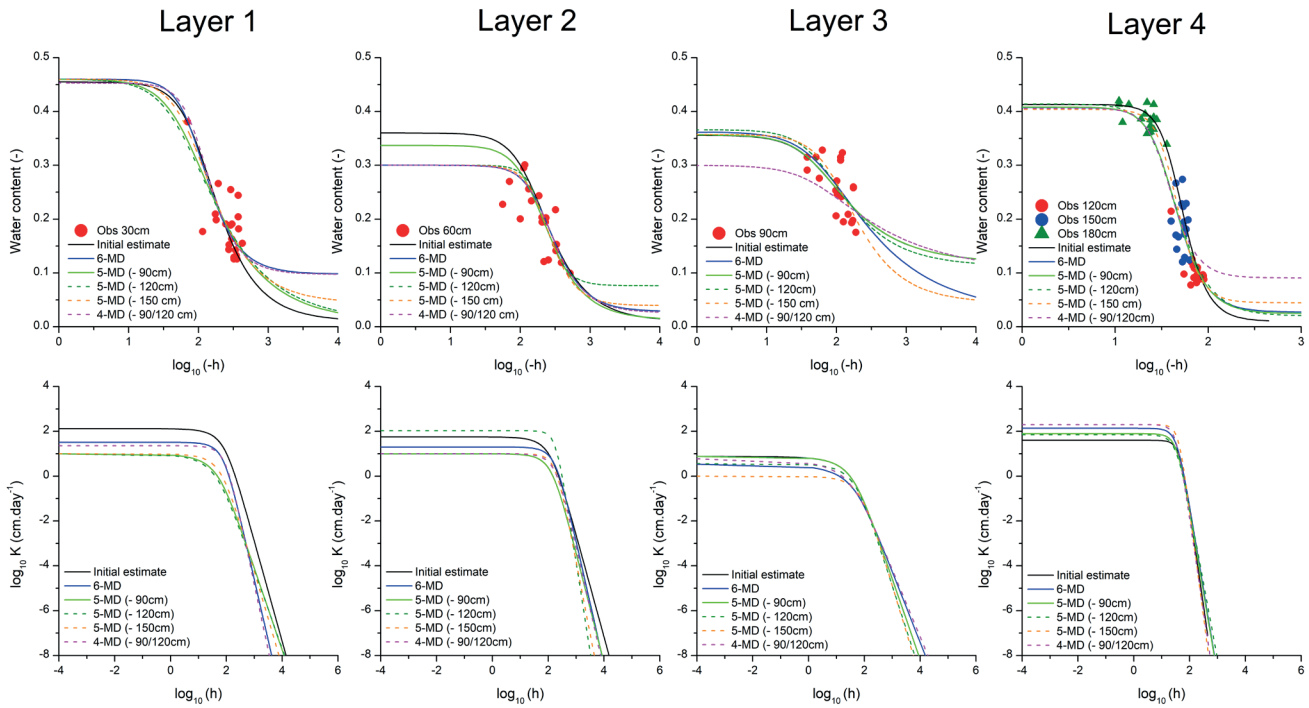

Figure 6. Soil water retention and hydraulic conductivity curves predicted by Rosetta (initial estimate) and each inverse modeling monitoring scheme: with all 6 sampling depths (6-MD) and the best fit scenarios with five (5-MD) and four (4-MD) sampling depths. The numbers in parentheses indicate the sampling depth excluded in each scheme. Field retention data, $\theta(h)$ is shown as red dots for each sampling depth and corresponding soil layer.

predicted SWS was 427 mm (7.2% lower than observed value). The rest of the illustrated cases in Fig. 5 shows good agreement with field measurements.

Soil hydraulic properties estimation uncertanties

Figure 6 shows predicted SWRC and hydraulic conductivity curve for the four layers of the soil profile. SWRC are compared with measured field retention data, 18 *θ(h)* measurements at each observation depth. Only the monitoring strategies that had a satisfactory model performance are presented. The field estimates of the SHP predicted by Rosetta were also included for comparative reasons. The observation points that had less weight in parameter prediction and could be potentially suppressed from the inverse objective function were 90 cm, 120 cm, 150 cm for 5-MD strategy and the combination of 90 cm and 120 cm for 4-MD strategy. Generally, the inversely predicted SHP could represent the variability of field retention data points by visual inspection. Agreement between measured and predicted θ by the SWRCs at specific h was quantified by the rRMSE (Table 6). All the proposed strategies presented a rRMSE lower than 0.30 in each soil layer. Thus, SHP estimation can be assumed acceptable. The global rRMSE for all layers together was 0.18 for the 6-MD and 5-MD cases and 0.20 for the 4-MD strategy. The field measured SWRCs had worse performance than SWRCs estimated by inverse modeling.

In layer 1, all the predicted SWRC showed similar patterns and the major difference between curves is the prediction of the parameter θ_r. Since retention data acquired in field by tensiometers are in the range of pressure heads from 0 to -1000 cm, this effect is not surprising and could explain that difference. The pressure heads needed to measure θ_r accurately are far beyond the measurement range of the equipment; even more, the proximity of the water table prevents the existence of very low values of *h*. Similar conditions are present in the rest of the layers. In layer 2, a discrepancy between curves is seen for the case of 5-MD when data from 90 cm were not considered. In this case, θ_s was greater (0.337 cm^3 cm^{-3}) than the other cases (0.3 cm^3 cm^{-3}). However, the variability of the predicted θ in the range of h measured in field is minimum.

As the observation points that could be removed corresponded to the layers 3 and 4, some uncertainties in SWRC prediction for each layer could be expected. Nevertheless, only in the 4-MD strategy the predicted curve differs slightly more in relation to the 6-MD scenario. For the layer 3 and 4, the values of θ_s and θ_r were underestimated and overestimated, respectively. In any manner, simulation of θ and h still represented reasonable the real data when the information of 90 and 120 cm was suppressed. As these observation points corresponded to the intermediate zone of the soil profile, they have a minor importance in the prediction of water fluxes. If data from the extreme layers are available, both upper and lower boundaries, θ and h from the middle section of the profile could be predicted anyway.

Table 6. Goodness of fit (relative root mean square error, rRMSE) for measured and predicted water content (by use of the soil water retention curves, SWRCs) at specific pressure heads predicted by Rosetta (initial estimate) and each inverse modeling monitoring scheme: with all 6 sampling depths (6-MD) and the best fit scenarios with five (5-MD) and four (4-MD) sampling depths. The numbers in parentheses indicate the sampling depth excluded in each scheme.

Layer	rRMSE					
	Rosetta	6-MD	5-MD (-90 cm)	5-MD (-120 cm)	5-MD (-150 cm)	4-MD (-90&120 cm)
1	0.204	0.183	0.177	0.174	0.182	0.193
2	0.229	0.187	0.205	0.194	0.190	0.188
3	0.251	0.248	0.251	0.251	0.255	0.294
4	0.126	0.108	0.108	0.110	0.104	0.118
All	0.202	0.182	0.185	0.182	0.183	0.198

Discussion

According to Ket *et al.* (2018), SHP can be correctly and rapidly estimated by inverse modeling using only soil water states (*i.e.,* θ and h) without the requirement of expensive laboratory data. In such a case, the definition of the monitoring strategy to best capture the hydrodynamic of soil water becomes essential. However, results showed that SHP optimized by inverse modelling varied according to the available data from different depths in the soil profile. Predicted water fluxes are uncertain to some degree, due to parameterization problems during calibration. Abbaspour *et al.* (1999) explained that parameters obtained by an inverse analysis are always statistically conditioned by factors such as the type and quality of the variables used in the objective function and the mathematical formulation of this objective function. Thus, monitoring strategies and experimental setup plays an important role in SHP optimization by inverse modeling. According to Valdes-Abellan *et al.* (2019) the combinations of SHP that better reproduce the observed data (even if those parameters do not fit accurately the experimental value) are preferable than combinations of SHP that better fit the real soil parameter value but do not reproduce the observed data. The selection of the monitoring strategy should be based on the research objective and the resources available to acquire the information, assessing both the time and economical cost related to the task (Valdes-Abellan *et al.*, 2015). Musters & Bouten (2000) probed numerical simulations offer quantitative means to distinguish efficiencies of different measurement strategies for model calibration. In calibration of a root uptake model, authors state that the installation depths of sensors are critical when fewer probes are used, and well-chosen depths are preferable to random or interval sampling schemes.

For the case study, the best fit between observed and predicted θ and h was achieved when field measurements were available for the greatest number of observation points. Nevertheless, the model performance was still very satisfactory for some monitoring strategies when one or two depths were suppressed from the inverse objective function. Compared to the best 6-MD scheme, deterioration of statistics EF and rRMSE for the 5-MD or 4-MD strategies was lesser than 10% and even lesser than 5% in some strategies. Also, visual inspection and the rRMSE asseverate that SWRC inversely predicted with less information still represents well the field retention data, θ (h). θ and h variables should be measured over time and in several depths to identify more precisely the SHP. However, due to diverse reasons, data acquisition is often limited, and it might be important to know which vertical depth should be unavoidably monitored to obtain correct estimates.

The observation points that had less weight in parameter prediction corresponded to the intermediate vadose zone. Additionally, if the removed data correspond to a layer with another observation point such as the case of the removal of 120 and 150 cm, the deterioration becomes smaller. When θ and h measurements from the upper and lower layers of the soil are available, θ and h from the middle section could be reasonably predicted by the model. This is valid, as the shallow water table directly influenced the water fluxes in the soil profile. The water table position is significant for the vertical distribution of θ and h (Tan *et al.*, 2014). The data from the two upper monitoring depths were important to define the variation in θ and h related the atmospheric condition. However, the monitoring depth closest to the phreatic aquifer was important to define the capillary fringe and its effects over soil water hydrodynamics. For future studies it is necessary to probe that this fact is valid for deeper vadose zones. In such cases by flowing deeper into the soil, the role of capillary force might be reduced and the main force for water movements are the atmospheric conditions (Altafi Dadgar *et al.*, 2020). It could be hypothesized in such a case, that the importance of deep sensors would be small and that they could be removed from the monitoring strategy without the loss of important information. In any case, the distribution of vertical sensors in the field must be modified according to the boundary conditions of the profile.

In the inverse modeling procedure, prior information of textural fractions and bulk density of soil layers were used to estimate the initial SHP. Scharnagl *et al.* (2011) demonstrated that prior information significantly improved parameter identifiability in inverse modeling and that in-situ θ measurements did not contain by themselves sufficient information to ensure a precise estimation of SHP. Therefore, is advisable to characterize the physical properties of the soil in detail, even if θ and h are not being monitored at a particular depth. Another option to reduce the uncertainties in SHP estimation is to set some parameters to some a priori defined values (Ritter *et al.*, 2003). The inverse modeling could be combined with other laboratory parameter determination techniques (*e.g.*, pressure plate extractor, hanging water column method, etc.). Thus, reducing the number of parameters optimized by the objective function and model uncertainties. Groh *et al.* (2018) estimated θ_s by other means to reduce the number of optimization parameters. Same, Thomas *et al.* (2017) fixed θ_r as it deemed insensitive to water content calibration. Also, K_s can be easily determined by direct field measurements (*e.g.*, permeameter, double-ring infiltrometer, minidisk infiltrometer, etc.). As shown previously, the inverse estimation of K_s for the upper soil layers predicted lower values than those measured in the field. Macropores may have influenced field measurement of Ks, mostly in the topsoil layers. As water movement was simulated for the single-porosity van Genuchten-Mualem hydraulic model discrepancies could appear in the estimation of Ks. Da Silva *et al.* (2020) indicate that the conventional way of parameterizing SHP comprises pressure plate apparatus for $\theta(h)$ and K(h), permeameter for K_s and l = 0.5. However, sometimes direct measurements poorly defined SHP and should be inevitably considered as fitting parameters (Scharnagl *et al.*, 2011). The monitoring strategy must be design based on the objectives of the research, considering both, the prior information of the profile and the resources available to acquire new data.

According to our results, inverse modeling allowed to identify the best monitoring strategies to obtain an accurate hydraulic model with a limited number of observations depths. Although, the best fit between observed and predicted θ and h was achieved for the scenario with the greatest number of observation points (6-MD), the model performance was still very satisfactory when one or two depths were suppressed from the dataset. Deterioration of statistics EF and RMSE in the proposed 5-MD or 4-MD strategies was lesser than 10% in comparison with the 6-MD scheme. The observation points that had less importance in parameter prediction corresponded to the intermediate vadose zone and to the layers with more observation depths. If data from the upper and lower boundaries of the soil profile are available, θ and h from the middle section could be predicted reasonably well. The inversely model SHP from the 5-MD and 4-MD strategies correctly represent field retention data points, $\theta(h)$. The monitoring schemes proposed in this work could be used in soil profile with similar conditions, and specially in experimental sites with a shallow water table. By reducing the number of vertical observations in the profile without harming the final estimates of the inverse modeling, the efficiency of field monitoring tasks can be greatly enhanced.

References

Abbaspour KC, Sonnleitner MA, Schulin R, 1999. Uncertainty in estimation of soil hydraulic parameters by inverse modeling: example lysimeter experiments. Soil Sci Soc Am J 63: 501-509. https://doi.org/10.2136/sssaj1999.03615995006300030012x

Allen RG, Pereira LS, Raes D, Smith M, 1998. Crop evapotranspiration. FAO Irrig & Drain Paper N° 56:

Altafi Dadgar M, Nakhaei M, Porhemmat J, Eliasi B, Biswas A, 2020. Potential groundwater recharge from deep drainage of irrigation water. Sci Total Environ 716: 1-12. https://doi.org/10.1016/j.scitotenv.2020.137105

Blake GR, Hartge KH, 1986. Bulk density. In: Methods of soil analysis, Part 1-Physical and mineralogical methods; Klute A (Ed.). SSSA Book Series, Madison, pp. 363-382. https://doi.org/10.2136/sssabookser5.1.2ed.c13

Bordoni M, Bittelli M, Valentino R, Chersich S, Meisina C, 2017. Improving the estimation of complete field soil water characteristic curves through field monitoring data. J Hydrol 552: 283-305. https://doi.org/10.1016/j.jhydrol.2017.07.004

Brooks RH, Corey AT, 1964. Hydraulic properties of porous media: hydrology papers. Colorado State University, Fort Collins.

Cornelis WM, Khlosi M, Hartmann R, van Meirvenne M, De Vos B, 2005. Comparison of unimodal analytical expressions for the soil-water retention curve. Soil Sci Soc Am J 69(6): 1902-1911. https://doi.org/10.2136/sssaj2004.0238

Da Silva AJP, Pinheiro EAR, de Jong van Lier Q, 2020. Determination of soil hydraulic properties and its implications for mechanistic simulations and irrigation management. Irrig Sci 38: 223-234. https://doi.org/10.1007/s00271-020-00664-5

Dane JH, Topp CG, 2002. Methods of soil analysis, Part 4: Physical methods. John Wiley & Sons. https://doi.org/10.2136/sssabookser5.4

Durner W, 1994. Hydraulic conductivity estimation for soils with heterogeneous pore structure. Water Resour Res 30: 211-223. https://doi.org/10.1029/93WR02676

Feddes RA, Bresler E, Neuman SP, 1974. Field test of a modified numerical model for water uptake by root

systems. Water Resour Res 10: 1199-1206. https://doi.org/10.1029/WR010i006p01199

Filipović V, Mallmann FJK, Coquet Y, Šimůnek J, 2014. Numerical simulation of water flow in tile and mole drainage systems. Agric Water Manage 146: 105-114. https://doi.org/10.1016/j.agwat.2014.07.020

Fredlund DG, Xing A, 1994. Equations for the soil-water characteristic curve. Can Geotech J 31(4): 521-532. https://doi.org/10.1139/t94-061

Gabriel JL, Quemada M, Martín-Lammerding D, Vanclooster M, 2019. Assessing the cover crop effect on soil hydraulic properties by inverse modelling in a 10-year field trial. Agric Water Manage 222: 62-71. https://doi.org/10.1016/j.agwat.2019.05.034

Gee GH, Bauder JW, 1986. Particle size analysis, 2nd ed. Methods of Soil Analysis, Part 1-Physical and Mineralogical Methods. SSSA Book Series, Madison.

Graham SL, Srinivasan MS, Faulkner N, Carrick S, 2018. Soil hydraulic modeling outcomes with four parameterization methods: comparing soil description and inverse estimation approaches. Vadose Zone J 17: 170002. https://doi.org/10.2136/vzj2017.01.0002

Groenevelt PH, Grant CD, 2004. A new model for the soil-water retention curve that solves the problem of residual water contents. Eur J Soil Sci 55: 479-485. https://doi.org/10.1111/j.1365-2389.2004.00617.x

Groh J, Stumpp C, Lücke A, Pütz T, Vanderborght J, Vereecken H, 2018. Inverse estimation of soil hydraulic and transport parameters of layered soils from water stable isotope and lysimeter data. Vadose Zone J 17(1): 1-19. https://doi.org/10.2136/vzj2017.09.0168

Guo X, Sun X, Ma J, Lei T, Zheng L, Wang P, 2018. Simulation of the water dynamics and root water uptake of winter wheat in irrigation at different soil depths. Water 10: 1033. https://doi.org/10.3390/w10081033

Hulsemann J, 1966. On the routine analysis of carbonates in unconsolidated sediments. J Sediment Res 36 (2): 622-625.

Ket P, Oeurng C, Degré A, 2018. Estimating soil water retention curve by inverse modelling from combination of in situ dynamic soil water content and soil potential data. Soil Syst 2: 1-23. https://doi.org/10.3390/soilsystems2040055

Khlosi M, Cornelis WM, Douaik A, van Genuchten MT, Gabriels D, 2008. Performance evaluation of models that describe the soil water retention curve between saturation and oven dryness. Vadose Zone J 7(1): 87-96. https://doi.org/10.2136/vzj2007.0099

Kosugi K, 1999. General model for unsaturated hydraulic conductivity for soils with log-normal pore-size distribution. Soil Sci Soc Am J 63: 270-277. https://doi.org/10.2136/sssaj1999.03615995006300020003x

Legates DR, McCabe GJ, 1999. Evaluating the use of "goodness-of-fit" measures in hydrologic and hydroclimatic model validation. Water Resour Res 35: 233-241. https://doi.org/10.1029/1998WR900018

Marquardt DW, 1963. An algorithm for least-squares estimation of nonlinear parameters. J Soc Ind Appl Math 11: 431-441. https://doi.org/10.1137/0111030

Mualem Y, 1976. A new model for predicting the hydraulic conductivity of unsaturated porous media. Water Resour Res 12: 513-522. https://doi.org/10.1029/WR012i003p00513

Musters PAD, Bouten W, 2000. A method for identifying optimum strategies of measuring soil water contents for calibrating a root water uptake model. J Hydrol 227: 273-286. https://doi.org/10.1016/S0022-1694(99)00187-0

Musters PAD, Bouten W, Verstraten JM, 2000. Potentials and limitations of modelling vertical distributors of root water uptake of an Austrian pine forest on a sandy soil. Hydrol Process 14: 103-115. https://doi.org/10.1002/(SICI)1099-1085(200001)14:1<103::AID-HYP913>3.0.CO;2-5

Nash JE, Sutcliffe JV, 1970. River flow forecasting through conceptual models part I - A discussion of principles. J Hydrol 10: 282-290. https://doi.org/10.1016/0022-1694(70)90255-6

Qu W, Bogena HR, Huisman JA, Martinez G, Pachepsky YA, Vereecken H, 2014. Effects of soil hydraulic properties on the spatial variability of soil water content: evidence from sensor network data and inverse modeling. Vadose Zone J 13(12): 1-12. https://doi.org/10.2136/vzj2014.07.0099

Ramos TB, Goncalves MC, Martins JC, van Genuchten MT, Pires FP, 2006. Estimation of soil hydraulic properties from numerical inversion of tension disk infiltrometer data. Vadose Zone J 5(2): 684-696. https://doi.org/10.2136/vzj2005.0076

Ritter A, Hupet F, Muñoz-Carpena R, Lambot S, Vanclooster M, 2003. Using inverse methods for estimating soil hydraulic properties from field data as an alternative to direct methods. Agric Water Manage 59: 77-96. https://doi.org/10.1016/S0378-3774(02)00160-9

Schaap MG, Leij FJ, van Genuchten MTh, 2001. ROSETTA: a computer program for estimating soil hydraulic properties with hierarchical pedotransfer functions. J Hydrol 251: 163-176. https://doi.org/10.1016/S0022-1694(01)00466-8

Scharnagl B, Vrugt JA, Vereecken H, Herbst M, 2011. Inverse modelling of in situ soil water dynamics: Investigating the effect of different prior distributions of the soil hydraulic parameters. Hydrol Earth Syst Sci 15: 3043-3059. https://doi.org/10.5194/hess-15-3043-2011

Schelle H, Durner W, Schlüter S, Vogel HJ, Vanderborght J, 2013. Virtual soils: moisture measurements and their interpretation by inverse modeling. Vadose Zone J 12: 1-12. https://doi.org/10.2136/vzj2012.0168

Scherger LE, Zanello V, Lexow C, 2019. Evaluation of recharge as vector flow for solute transport in the industrial area of Bahía Blanca (Argentina). 2nd Int Conf on the Environment and 4th Nat Conf on the Environment, Tandil.

Scherger LE, Zanello V, Lexow C, 2020. Comparison of the inverse modeling approach and traditional methods to estimate the unsaturated hydraulic properties in a sandy loam soil. Revista Aguas Subterrâneas 34: 310-324. https://doi.org/10.14295/ras.v34i3.29929

Šimůnek J, Hopmans JW, 2002. Parameter optimization and nonlinear fitting. In: Methods of soil analysis: Part 4 Physical methods; Dane JH & Topp GC (Eds.). SSSA Book Series, pp. 139-157. https://doi.org/10.2136/sssabookser5.4.c7

Šimůnek J, van Genuchten MTh, Wendroth O, 1998. Parameter estimation analysis of the evaporation method for determining soil hydraulic properties. Soil Sci Soc Am J 62: 894-905. https://doi.org/10.2136/sssaj1998.03615995006200040007x

Šimůnek J, Šejna MA, Saito H, Sakai M, van Genuchten MTh, 2013. The HYDRUS-1D software package for simulating the movement of water, heat, and multiple solutes in variably saturated media, version 4.17.

Tan X, Shao D, Liu H, 2014. Simulating soil water regime in lowland paddy fields under different water managements using HYDRUS-1D. Agric Water Manage 132: 69-78. https://doi.org/10.1016/j.agwat.2013.10.009

Thomas N, Schilling KE, Amado AA, Streeter M, Weber L, 2017. Inverse modeling of soil hydraulic properties in a two-layer system and comparisons with measured soil conditions. Vadose Zone J 16(2): 1-14. https://doi.org/10.2136/vzj2016.08.0072

Too V, Omuto C, Biamah E, Obiero J, 2014. Review of soil water retention characteristic (SWRC): Models between saturation and oven dryness. Open J Modern Hydrol 4: 173-182. https://doi.org/10.4236/ojmh.2014.44017

Valdes-Abellan J, Jiménez-Martínez J, Candela L, Tamoh K, 2015. Comparison among monitoring strategies to assess water flow dynamic and soil hydraulic properties in agricultural soils. Span J Agric Res 13: e1201. https://doi.org/10.5424/sjar/2015131-6323

Valdes-Abellan J, Pachepsky Y, Martinez G, Pla C, 2019. How critical is the assimilation frequency of water content measurements for obtaining soil hydraulic parameters with data assimilation? Vadose Zone J 18(1): 1-10. https://doi.org/10.2136/vzj2018.07.0142

van Genuchten MTh, 1980. A closed-form equation for predicting the hydraulic conductivity of unsaturated soils. Soil Sci Soc Am J 44: 892-898. https://doi.org/10.2136/sssaj1980.03615995004400050002x

van Genuchten MTh, Leij FJ, Yates SR, 1991. The RETC code for quantifying the hydraulic functions of unsaturated soils. EPA 600: 2-91.

Ventrella D, Castellini M, di Prima S, Garofalo P, Lassabatère L, 2019. Assessment of the physically-based Hydrus-1D model for simulating the water fluxes of a Mediterranean cropping system. Water 11: 1-19. https://doi.org/10.3390/w11081657

Vereecken H, Weynants M, Javaux M, Pachepsky Y, Schaap MG, van Genuchten MT, 2010. Using pedotransfer functions to estimate the van Genuchten-Mualem soil hydraulic properties: A review. Vadose Zone J 9(4): 795-820. https://doi.org/10.2136/vzj2010.0045

Wang X, Li Y, Chen X, Wang H, Li L, Yao N, Liu DL, Biswas A, Sun S, 2021. Projection of the climate change effects on soil water dynamics of summer maize grown in water repellent soils using APSIM and HYDRUS-1D models. Comput Electron Agric 185: 106142. https://doi.org/10.1016/j.compag.2021.106142

Wesseling JG, 1991. Meerjarige simulatie van grondwaterstroming voor verschillende bodemprofielen, grondwatertrappen en gewassen met het model SWATRE. Rapport 152, Staring Centrum, Wageningen 1-63.

Yakirevich A, Gish TJ, Šimunek J, van Genuchten MTh, Pachepsky YA, Nicholson TJ, Cady RE, 2010. Potential impact of a seepage face on solute transport to a pumping well. Vadose Zone J 9: 686-696. https://doi.org/10.2136/vzj2009.0054

Yetbarek E, Kumar S, Ojha R, 2020. Effects of soil heterogeneity on subsurface water movement in agricultural fields: A numerical study. J Hydrol 590: 125420. https://doi.org/10.1016/j.jhydrol.2020.125420